Bifunctional Au@Pt/Au core@shell nanoparticles as novel electrocatalytic tags in immunosensing: application for Alzheimer's disease biomarker detection

Alba Iglesias-Mayor [a], Olaya Amor-Gutiérrez [a], Antonello Novelli [b, c, d], María-Teresa Fernández-Sánchez [c, e], Agustín Costa-García [a],Alfredo de la Escosura-Muñiz [a]*

[a] NanoBioAnalysis Group- Department of Physical and Analytical Chemistry, University of Oviedo, Julián Clavería 8, 33006, Oviedo, Spain

[b] Department of Psychology, University of Oviedo, Plaza Feijoo s/n, 33003, Oviedo, Spain

[c] University Institute of Biotechnology of Asturias (IUBA), University of Oviedo, Doctor Fernando Bongera s/n, 33006, Oviedo, Spain

[d] Health Research Institute of the Principality of Asturias (ISPA), Hospital Universitario s/n, 33011, Oviedo, Spain

[e] Department of Biochemistry and Molecular Biology, University of Oviedo, Doctor Fernando Bongera s/n, 33006, Oviedo, Spain

*Corresponding author: Dr. Alfredo de la Escosura-Muñiz, Phone: +34 98 510 35 21, E-mail address: alfredo.escosura@uniovi.es.

ABSTRACT: In this work, bifunctional core@shell Au@Pt/Au NPs are presented as novel tags for electrochemical immunosensing. Au@Pt/Au NPs were synthesized following a chemical route based on successive metal depositions and galvanic replacement reactions from the starting AuNPs. Au protuberances growth on the surface of Au@Pt NPs allowed their easy bioconjugation with antibodies, while the high catalytic Pt surface area was approached for their sensitive detection through the electrocatalysed water oxidation reaction (WOR) at neutral pH. Moreover, the synergy between Au and Pt metals on the NP surface also lead to an increased catalytic activity, improving the sensitivity of the NP detection. Cyclic voltammetry and chronoamperometry were used for the evaluation of the Au@Pt/Au NPs electrocatalytic activity towards WOR. The chronoamperometric current recorded at a fixed potential of +1.35 V was selected as the analytical signal, allowing the quantification of Au@Pt/Au NPs at 10^{13} NPs/mL levels. The optimized electrocatalytic method was applied to the quantification of conformationally altered p53 peptide Alzheimer's disease (AD) biomarker in a competitive immunoassay using magnetic bead (MB) platforms at levels as low as 66 nM. The performance of the system in a real scenario was demonstrated analysing plasma samples from a cognitively healthy subject. This novel Au@Pt/Au NPs-based electrocatalytic immunoassay has the advantage, over common methods for NP tags electrochemical detection, of the signal generation in the same neutral medium where the immunoassay takes place (0.1 M PBS pH 7.2), avoiding the use of additional and more hazardous reagents and paving the way to future integrated biosensing systems.

INTRODUCTION

The use of catalytic materials has attracted increasing attention in the last years. Of especial relevance are heterogeneous materials, which compared to homogenous materials provide more selectivity and a better yield [1]. At nanoscale, nanoparticle (NP) catalysts lead to higher catalytic activity than bulk materials due to their higher specific surface area [2].

NPs are promising candidates to be used as tags in biosensing assays. Compared to natural enzymes they show a more controlled synthesis, higher stability against harsh conditions, higher resistance to high concentrations of substrate and a lower cost [3–6]. The use of electrocatalytic NPs as labels has been extensively studied and applied in immunosensing [7–12], offering outstanding alternatives to traditional assays.

Among the wide variety of NPs, metallic NP labels have attracted considerable interest due to their unique red-ox and optical properties [13,14] as well as their electrocatalytic activity, also benefiting of the inherent advantages of the electrochemical detection in terms of sensitivity, selectivity, simplicity and low cost [15]. In most cases highly acidic media are needed for such NPs detection, either to facilitate dissolution [16] or as source of hydrogen ions for further detection based on hydrogen evolution reaction (HER) [17–23]. However, the use of acid solutions is not desirable for both safety reasons and the time needed for the analysis, also involving additional steps after the immunoassay.

Consequently, there is a need of NP tags that may be detected in the same medium where immunoreactions take place. In this context, the water oxidation reaction (WOR) occurring at neutral pH and easily catalysed by some metals emerges as an ideal tool for NPs detection [24]. WOR, also known as oxygen evolution reaction (OER), is a four-electron transfer reaction ($2\,H_2O \rightarrow O_2 + 4H^+ + 4e^-$) that takes places in the anode of an electrolytic cell. This reaction, together with HER, a two-electron cathodic process, ($2H^+ + 2e^- \rightarrow H_2$) is involved in

electrochemical water splitting [25]. It has been shown that an efficient water splitting can be achieved by Platinum (Pt), Ruthenium (Ru) and Iridium (Ir) based materials. It's also well known that Pt catalyses HER process in a high extent, whereas IrO_2 and RuO_2 show a remarkable activity towards WOR [26–31]. Pt has been extensively studied, mainly because of its electrocatalytic activity towards a wide variety of reactions, such as hydrogen evolution, oxygen reduction, hydrogen peroxide reduction, hydrogen oxidation, methanol oxidation, ethanol oxidation and formic acid oxidation [32,33]. Pt scarcity and high cost makes desirable its combination with other metals to reduce costs and to enhance its catalytic performance due to the synergistic effects between metals [34–38].

The loading of Pt on the surface of Au, as in core@shell Au@Pt NPs, has been extensively studied and excellent catalytic properties have been reported due to the aforementioned synergistic effect [39,40]. Based on their electrocatalytic activity towards reactions such as the hydrogen peroxide reduction and the oxygen reduction, Au@Pt NPs have been used as electrode modifiers in label-free immunosensors [41,42] and also as tags in aptasensors [43] and immmunosensors [44]. However, few information has been found regarding the synthesis of multi-layered bimetallic core@shell NPs, with two or more components exposed to the environment. Xie et al. [45]described for the first time the synthesis of raspberry-like bimetallic Au@Pt/Au triple-layered core@shell NPs consisting of an Au core, a Pt inner shell, and an outer shell composed of Au protuberances. Such Au@Pt/Au NPs showed peroxidase-like activity [46] but, to the best of our knowledge, no other catalytic properties have been evaluated yet.

In this context, here we explore for the first time the electrocatalytic properties of Au@Pt/Au NPs towards the WOR in neutral media and their use as tags in biosensing, taking advantage of the Au protuberances for antibody immobilization. The methodology was employed in a competitive magnetoimmunoassay for the detection of an altered conformation of the p53 peptide, a novel Alzheimer's disease (AD) biomarker. AD is one of the most common causes of dementia worldwide, affecting more than 47 million people [47]. The use of conformationally altered p53 as a biomarker for AD was proposed by Lanni et al. in 2007, who observed that fibroblasts from patients with AD expressed high levels of a conformationally altered (or unfolded) p53 peptide [48,49]. The new methodology we propose here, using Au@Pt/Au NPs as novel labels alternative to enzymes and with the advantage of easy detection in the same medium where the immunoreaction takes place, opens the way to further biomedical applications and integrated biosensing systems.

EXPERIMENTAL SECTION

Reagents and materials

The precursors used for the synthesis of the Au@Pt/Au NPs gold (III) chloride trihydrate ($HAuCl_4 \cdot 3\ H_2O$), silver nitrate ($AgNO_3$) and chloroplatinic acid solution (H_2PtCl_6), were obtained from Sigma-Aldrich (Spain). The reducing agent, trisodium citrate ($Na_3C_6H_5O_7 \cdot 2\ H_2O$), used during the synthetic and conjugation procedure was purchased from Merck (Germany).

Streptavidin-modified magnetic beads 2.8 µm-sized (M-280) and anti-p53 monoclonal antibody (PAb240) recognizing specifically conformationally altered p53 were purchased from Thermo Fisher Scientific (Spain). Conformationally altered p53 and biotin-conjugated conformationally altered p53 peptide were synthesized by Abyntek Biopharma (Spain).

All chemicals were of analytical grade and used as received without further purification. All the solutions were prepared in ultrapure water (18.2 MΩ·cm @ 25 ºC) directly taken from a Millipore Direct-Q® 3 UV purification system from Millipore Ibérica S.A (Spain). Unless otherwise stated, all buffer reagents and other inorganic chemicals were supplied by Sigma-Aldrich (Spain) or Merck (Germany). Phosphate buffer electrolyte solution was prepared using sodium chloride, potassium chloride, disodium hydrogen phosphate and potassium dihydrogen phosphate from Merck (Germany). Blocking buffer (BB) solution consisted in 0.1 M PBS pH 7.2 solution with added 5% (w/v) bovine serum albumin. The binding and washing (B&W) buffer consisted in 0.1 M PBS pH 7.2 solution with 0.05% (v/v) Tween®-20.

Instrumentation

A thermostatic centrifuge (Rotanta 460 R) from Hettich (Germany) was used to purify the Au@Pt/Au NPs and their antibody conjugates. An MSC-100 cooling thermo shaker incubator purchased from Labolan (Spain) was used for the incubations. A MagRack™ 6 purchased from Sigma-Aldrich (Spain) was used for the magnetic separations. UV-visible (UV-Vis) spectra were recorded with Genesys 10S UV-Vis Spectrophotometer from Thermo Scientific (United States of America). Nanoparticles Zeta potential was determined by Dynamic light scattering (DLS) using a Zetasizer Nano ZS system from Malvern Instruments (United Kingdom). High resolution-transmission electron microscopy (HR-TEM) images were obtained using a FEI Tecnai G^2 F20 S-TWIN field-emission gun high resolution microscope from FEI (United States of America) on a copper grid, using an accelerating voltage of 200 kV. Electrochemical measurements were performed with an Autolab PGSTAT-10 from Eco Chemie (Netherlands), controlled by Autolab GPES software from Metrohm (Switzerland). Both screen-printed carbon electrodes (SPCEs, ref. DRP-110) and their connector to the potentiostat (ref. DRP-DSC) were purchased from Metrohm DropSens S.L (Spain). The conventional three-electrode configuration of SPCEs includes both carbon working and counter electrodes and a silver pseudoreference electrode. A magnetic support for SPEs (DRP-MAGNET-700) also from Metrohm DropSens S.L (Spain) was used to perform the measurements with the magnetic beads.

Synthesis, bioconjugation and characterization of Au@Pt/Au NPs

Synthesis of bifunctional Au@Pt/Au NPs was performed as previously described [45] with some modifications. Briefly, 80 mL of an aqueous 2.94×10^{-4} M gold (III) chloride trihydrate solution were reduced by 2 mL of an aqueous 3.88×10^{-2} M trisodium citrate solution at boiling point (the reaction temperature for all the following NP synthetic steps) under vigorous magnetic stirring for 30 min, obtaining AuNPs suspensions of 9.00×10^{14} NPs/mL, according with the method pioneered by Turkevich *et al.*[50]. Then, 3 mL of an aqueous 5.88×10^{-3} M silver nitrate solution were added dropwise to 51.25 mL of stirred AuNPs solution, and, subsequently 750 µL of the aqueous 3.88×10^{-2} M trisodium citrate solution were added. After 1 h under vigorous magnetic stirring at boiling point, 80 µL of an aqueous 1.95×10^{-1} M chloroplatinic acid solution were added

and immediately a dark mauve colloid was obtained. The product was centrifuged, and the pellet was resuspended in ultrapure water. Then, 1.2 mL of the aqueous 5.88×10^{-3} M silver nitrate solution were added to 45 mL of Au@Pt NPs solution at the same heating and stirring conditions as before, and, subsequently, 300 µL of the aqueous 3.88×10^{-2} M trisodium citrate solution were added. Again, the reaction mixture was left boiling for 1 h. For the final gold growing step, 150 µL of the aqueous 2.94×10^{-4} M gold (III) chloride trihydrate and 150 µL of the aqueous 3.88×10^{-2} M trisodium citrate solutions were added simultaneously to the Au@Pt@Ag NPs suspension and the reaction was stopped after 20 min, leading to the formation of the Au@Pt/Au NPs. All the NPs solutions were stored at 4 °C.

The synthesized Au@Pt/Au NPs were then conjugated with anti-p53 monoclonal antibody following a well-known methodology for AuNPs conjugation[13]. Briefly, 1.5 mL of the NPs suspension (9.00×10^{14} NPs/mL) was centrifuged at 7500 g at 20 °C for 30 min in presence of 0.025% (v/v) Tween®-20. The supernatant was removed, and the pellet was resuspended in 2 mM trisodium citrate pH 7.5 to the original volume. After that, 1.4 mL of the resuspended solution was mixed with 115 µL of 100 µg/mL anti-p53 and incubated at 25 °C for 60 min with stirring (700 rpm). Finally, the solution was centrifuged at 7500 g at 4 °C for 30 min, the supernatant was removed and the purified Au@Pt/Au NPs/anti-p53 pellet was re-dispersed in 1.4 mL of aqueous 1% (w/v) bovine serum albumin (BSA) solution, obtaining 1.4 mL of Au@Pt/Au NPs/anti-p53 conjugate containing approximately 9.00×10^{14} NPs/mL.

High resolution-transmission electron microscopy, UV-Vis absorbance spectroscopy and dynamic light scattering were used for characterizing the NPs obtained in each step of the synthesis route.

Electrochemical measurements

Each electrochemical measurement was performed after dropping 40 µL of NPs suspension in 0.1 M PBS pH 7.2 onto the SPCE surface and keeping there for 30 seconds. Background signals were recorded following the same electrochemical procedure but using an aliquot of 0.1 M PBS pH 7.2. Cyclic voltammetry scans were recorded in the range from +0.10 V to +1.35 V at a scan rate of 50 mV/s. Chronoamperometric scans were performed holding the working electrode at a fixed potential of +1.35 V for 300 s. The electrocatalysed oxidation reaction was chronoamperometrically followed measuring the current generated during the time. The absolute value of the current at 300 s was chosen as the analytical signal.

For all the experiments, the measurements were made by triplicate at room temperature. Removing oxygen from the solution was not necessary. A new SPCE was used for each measurement.

Competitive immunoassay for conformationally altered p53 Alzheimer's disease biomarker detection

A magnetic bead (MB)-based competitive immunoassay was performed for conformationally altered p53 peptide quantification. Briefly, 150 µg (15 µL from the stock solution) of streptavidin-modified MBs was transferred into 0.5mL Eppendorf tube. The MBs were washed twice with 150 µL of B&W buffer. The MBs were then resuspended in 108 µL of B&W buffer, and 42 µL of 1.0 mg/mL solution of biotinylated p53 (p53-Biotin) were added. The resulting MB and p53-Biotin solution was incubated for 30 min at 25 °C with gentle mixing (700 rpm) in the thermo shaker incubator. The formed MB/p53 complex was then separated from the incubation solution, using a MagRack™, washed 3 times with 150 µL of B&W buffer, and resuspended in 150 µL of blocking buffer (PBS–BSA 5%) followed for a 1h incubation at 25 °C under gentle stirring (700 rpm) so as to block any remaining active surface of MBs and to avoid unspecific absorptions.

In parallel, 144 µL of the Au@Pt/Au NPs/anti-p53 conjugate (approx. 9.00×10^{14} NPs/mL) was incubated for 1 h at 25 °C under gentle stirring (700 rpm) with 16 µL of solutions with different concentrations of conformationally altered p53 protein in the range 50-1000 nM (PBS or human IgG, for the blank and negative control assays respectively). After that, 150 µL of the resulting Au@Pt/Au NPs/anti-p53/p53 complex was incubated for 60 min with the blocked MB/p53 (after triple washing with B&W buffer) in the same conditions of temperature and stirring as before.

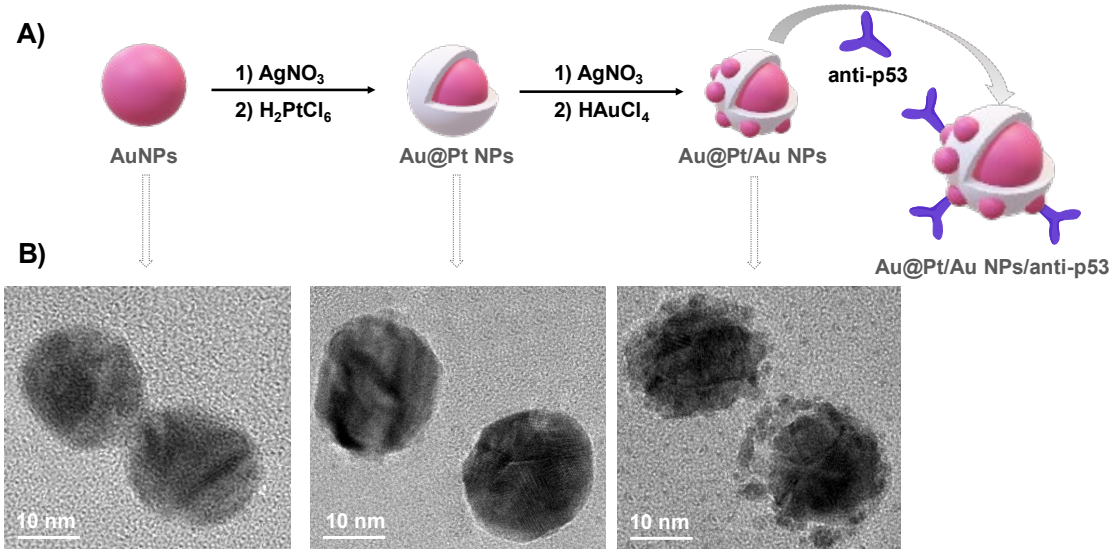

The resulting magnetoimmunocomplex was magnetically separated from solution, two times washed in B&W buffer, two times in PBS solution and then reconstituted in 150 µL of 0.1 M PBS pH 7.2. Finally, the p53 linked to the MBs, and captured through the immunoassay was electrochemically evaluated through the water oxidation reaction catalysed by the Au@Pt/Au NPs. Electrochemical measurements were performed following the experimental procedure described previously, using 40 µL of the immunocomplex suspension instead of the NPs solution, and using a magnetic support for SPCEs.

Spike and recovery protocol

Spike and recovery experiment is an important method for validating and assessing the accuracy of an analytical technique in complex matrixes. It was performed to determine whether conformationally altered p53 quantification is affected by a real sample matrix (plasma) when compared with the diluent (PBS) used to prepare the standard curve. A plasma sample from a cognitively healthy subject, kindly provided by the Neurology Unit of Cabueñes Hospital (Gijón, Asturias, Spain), was used for such purpose.

This experiment was performed by spiking the plasma sample with different concentrations (100, 500 y 1000 nM) of conformationally altered p53 protein (n=3 for each sample). Then, the spiked sample was electrochemically evaluated in the immunoassay. After that, the % recovery of the analytical signal in the real matrix sample was calculated.

RESULTS AND DISCUSSION

Synthesis and characterization of Au@Pt/Au NPs

Bifunctional core@shell Au@Pt/Au NPs were prepared following a previously optimized procedure based on successive metal depositions and galvanic replacement reactions from an AuNP starting core [45], as illustrated in Figure 1A. The first step consisted in the formation of an Ag shell around the AuNP core by chemical reduction of silver nitrate by sodium citrate, followed by the substitution of Ag by Pt via galvanic replacement using chloroplatinic acid. Then silver was deposited on the Pt surface using the same reagents than in the first coating. Finally, Au@Pt/Au NPs were obtained through the concerted action of both reagent reduction and galvanic replacement, leading to the formation of Au protuberances rather than a complete and smooth Au shell. The total replacement of Ag in the NPs was previously demonstrated by energy-dispersive X-ray (EDX) spectroscopy analysis [45]. The conjugation of anti-p53 monoclonal antibody onto the Au@Pt/Au NPs was then performed, taking advantage of the Au protuberances on the surface of the NPs through the well-known affinity of antibody cysteine groups to gold substrates [13].

The high resolution-transmission electron microscopy (HR-TEM) images obtained after each step of the synthetic route (Figure 1B) demonstrated the successful synthesis of first 17-nm sized spherical AuNPs, the subsequent formation of 19-nm sized spherical core@shell Au@Pt NPs, and the final generation of Au protuberances on their surface, leading to the Au@Pt/Au NPs obtaining.

The monodispersity of the Au@Pt/Au NPs is well observed in the HR-TEM image shown in Figure 2A. The corresponding size distribution histogram (n=150) depicted in the same figure gave a nanoparticle average diameter of 23 ± 2 nm.

NPs were also characterized by UV-Vis absorbance spectroscopy and dynamic light scattering (DLS) analysis. UV-Vis spectra were recorded between 400 and 650 nm (Figure 2B, left), finding that the starting AuNPs maximum absorbance wavelength (519 nm) shifted to higher values when advancing in the synthesis process. This behaviour is in agreement with previous studies demonstrating a gradual change in the covering of the starting NPs [39]. A further red-shift was observed when the final Au@Pt/Au NPs were modified with antibodies. Such shift is attributed to changes in the NPs surface plasmon resonance, and suggests the formation of the NP/antibody conjugates, also in agreement with previous reports [51].

Zeta potential measurements were conducted to determine the stability of the NP suspensions and to corroborate the bioconjugation of the Au@Pt/Au NPs with the anti-p53 antibody (Figure 2B, right).The Zeta potential values between -37 and -27 mV obtained for the different NPs (Au, Au@Pt and Au@Pt/Au NPs), corroborated the stability of the synthesized NP suspensions, as it is known that NP aggregation is avoided at absolute zeta potential values higher than 10 mV [51]. The Zeta potential shifted to a less negative value (-20 mV) after the bioconjugation of the Au@Pt/Au NPs, evidencing the substitution of the citrate ions on the external Au surface by the antibodies, and the formation of negatively charged stable conjugates.

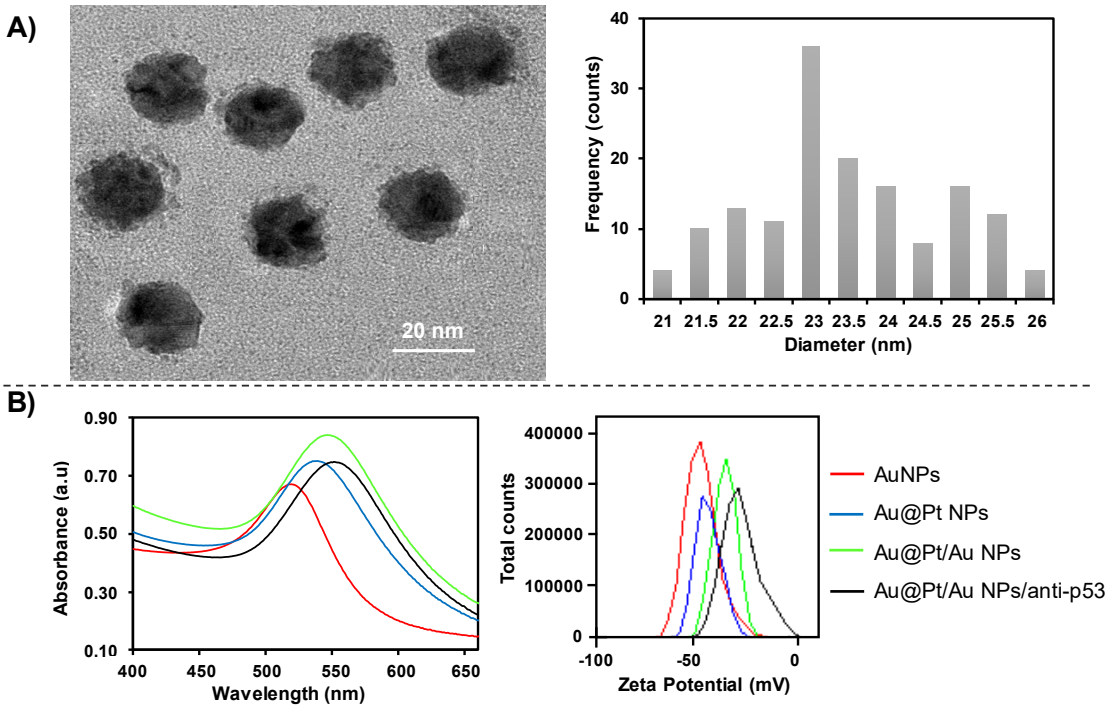

Figure 2. (**A**) (left) HR-TEM micrograph and (right) nanoparticle size distribution histogram of the obtained Au@Pt/Au NPs. (**B**) (left) UV-Vis spectra and (right) diagram for the Zeta potential as a distribution versus total counts, for AuNPs (red line), Au@Pt NPs (blue line), Au@Pt/Au NPs (green line) and Au@Pt/Au NPs/anti-p53 (black line).

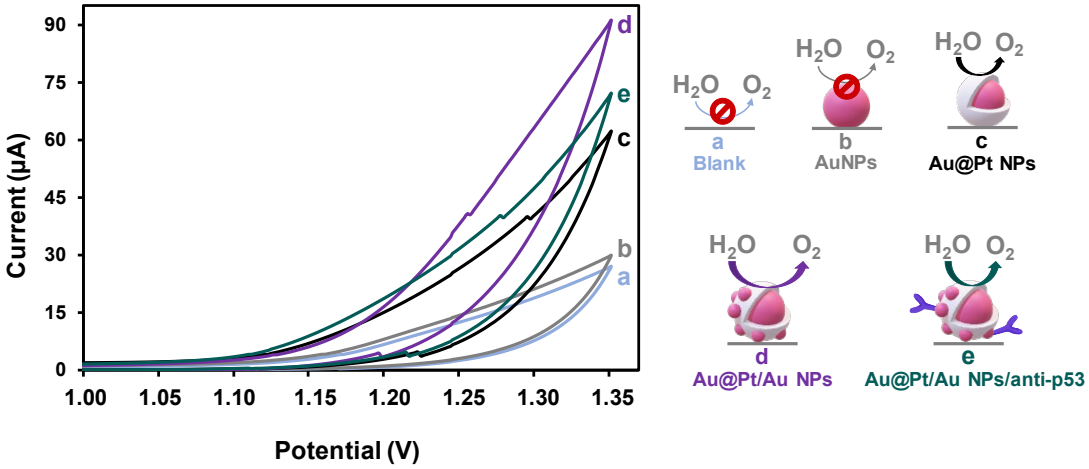

Figure 3. Cyclic voltammograms recorded from +0.10 to +1.35 V at a scan rate of 50 mV/s for 0.1 M PBS pH 7.2 solutions without NPs (blank) (a) and containing 9.00×10^{14} NPs/mL suspensions of: AuNPs (b), Au@Pt NPs (c), Au@Pt/Au NPs (d) and Au@Pt/Au NPs/anti-p53 (e).

The electrocatalytic activity of the different NPs towards the water oxidation reaction (WOR) was first evaluated by cyclic voltammetry (CV) on SPCEs. Cyclic voltammograms (CVs) were recorded from +0.10 V to +1.35 V in 0.1 M PBS pH 7.2. CV scans for the Au@Pt/Au NPs, both bare and bioconjugated, as well as those for their synthetic precursors (Au and Au@Pt NPs) are shown in Figure 3.

The background (curve a) shows that the oxidation of the medium´s oxygen started at around +1.15 V. The water oxidation profile remained almost constant in presence of AuNPs (curve b), evidencing that these NPs don't exert any effect towards this reaction, as expected. Interestingly, the presence of the platinum layer in the Au@Pt NPs shifted the half-wave potential of the WOR to less positive values (40 mV), from +1.305 V to +1.265 V, also noticing a high increase in the current (35 µA) recorded at +1.35 V (curve c). This behaviour suggests a high catalytic effect of the Pt towards the WOR. The origin of such effect may be related to the stabilization of the $4H^+/4e^-$ intermediates involved in the WOR, previously observed for different metals. This stabilization results in a lower kinetic barrier and, consequently, faster rates of oxygen production [29].

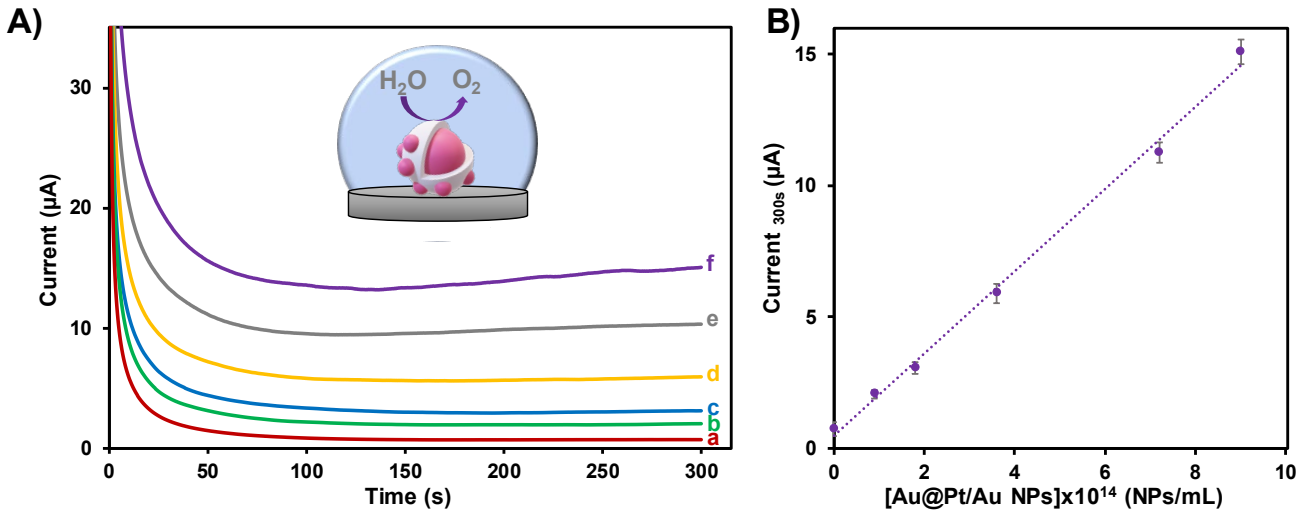

Figure 4. (**A**) Chronoamperograms recorded at +1.35 V during 300 s for 0.1 M PBS pH 7.2 without NPs (blank) (a) and containing increasing concentrations of Au@Pt/Au NPs: 9.00×10^{13} (b), 1.80×10^{14} (c), 3.60×10^{14} (d), 7.20×10^{14} (e) and 9.00×10^{14} NPs/mL (f). (**B**) Relationship between the analytical signal and NP concentration. Data are given as average ± SD (n=3).

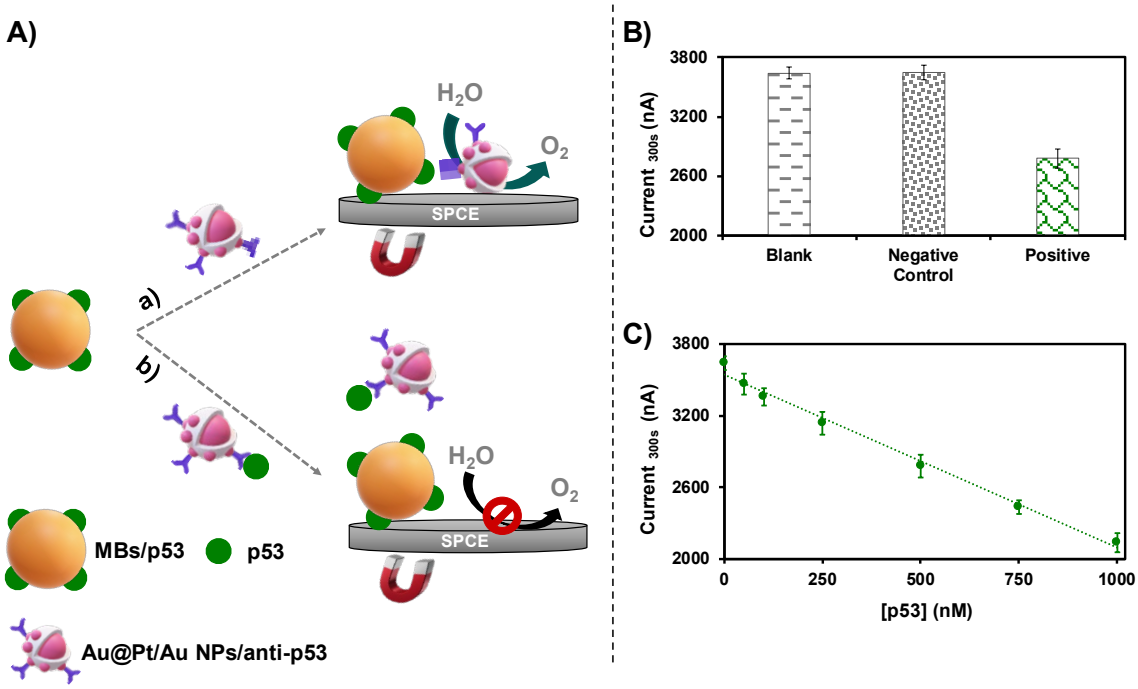

conformationally altered p53 AD biomarker detection using Au@Pt/Au NP tags. (**B**) Analytical signals obtained for 0.1 M PBS pH 7.2 solutions without protein ("blank") and containing 500 nM human IgG ("negative control") or 500 nM of p53 ("positive"); (**C**) Relationship between the analytical signal and conformationally altered p53 concentration (from 50 to 1000 nM). Data are given as average ± SD (n=3).

This effect was notably more relevant for the Au@Pt/Au NPs for which a potential shift of 55 mV and a current increase of 65 µA (curve d) was observed. These results suggest a synergistic effect between Au and Pt, leading to an increased catalytic activity. This behaviour was also expected, such the synergy in the catalytic activity of bimetallic NPs is a well-known feature, extensively studied in chemical synthesis procedures among other reactions [34–38], and being also found for Au@Pt NPs [39,40].

The evaluation of the Au@Pt/Au NPs activity after conjugation with antibodies is of key relevance for the further biosensing application. As observed in curve e, such conjugate retained most of the catalytic activity, allowing for its use as an electrochemical tag. The little decrease in activity compared with bare Au@Pt/Au NPs could be attributed to a partial blocking of the Au surface by the antibodies, which might somehow affect the synergy between both metals.

Chronoamperometric mode was chosen for the quantification of Au@Pt/Au NPs due to its high sensitivity, simplicity and speed. A fixed potential of +1.35 V was used in these experiments, at which a steady-state current was reached. As observed in Figure 4A, increasing NP concentrations in the range from $9.00x10^{13}$ to $9.00x10^{14}$ NPs/mL led to an increase in the catalytic current.

The analytical signal was extracted from the chronoamperograms as the current recorded at 300 seconds (current profiles were not stable for shorter times). As shown in Figure 4B, a linear relationship between the analytical signal and the Au@Pt/Au NPs concentration was found in the range between $9.00x10^{13}$ and $9.00x10^{14}$ NPs/mL adjusted to the following equation:

$$Current_{300s}\ (\mu A) = 1.57x10^{-14}\ [Au@Pt/Au\ NPs]\ (NPs/mL) + 0.5$$

The calibration curve showed a good correlation coefficient (r=0.9987) and reproducibility, with relative standard deviations (RSD) comprised between 2.4 and 5.2% (n=3). The limit of detection (LOD, calculated as three times the standard deviation of the intercept divided by the slope) was found to be $5.00x10^{13}$ NPs/mL.

Electrocatalytic detection of conformationally altered p53 Alzheimer's disease biomarker using Au@Pt/Au NP tags

Conformationally altered p53 peptide Alzheimer's disease biomarker was selected as the analyte to be used in the proof-of-concept. The competitive immunoassay for the determination of this peptide developed using Au@Pt/Au NP tags and magnetic bead (MB) platforms is schematized in **Figure 5A**. The use of MBs has well-known advantages related to the preconcentration of the samples and minimization of matrix effects, as well as to the reduction of the time of analysis. Briefly, biotinylated p53 was immobilized on the streptavidin-modified MBs, forming the MB/p53 conjugate. In parallel, the sample containing the analyte was incubated with the Au@Pt/Au NPs/anti-p53 conjugate, and the resulting complex was added to the MB/p53 conjugate. In absence of p53 (a) the Au@Pt/Au NPs/anti-p53 conjugate is captured by the MBs/p53 one, producing a high catalytic current coming from the WOR electrocatalysed by the Au@Pt/Au NPs. In contrast, in the presence of p53 (b) the amount of conjugate captured by MBs-p53 decreases, leading to a decrease in the catalytic current.

The Au@Pt/Au NPs/anti-p53 conjugate containing approximately $9.00x10^{14}$ NPs/mL, prepared as detailed in the experimental section, was directly used in the competitive immunoassay for p53 detection. As in any competitive assay, we first evaluated the maximum signal given by the conjugate after reaction with the p53 immobilized on the magnetic beads (absence of analyte). The obtained current of approximately 4 µA ("blank" assay in **Figure 5B**) suggests that not signal saturation conditions are reached (currents up to 15 µA were obtained when analysing the NP suspensions, as seen in **Figure 4**), so further evaluation of lower amounts of the conjugate was not considered necessary.

The noticed difference between the current recorded in the Au@Pt/Au NPs quantification assay for a $9.00x10^{14}$ NPs/mL suspension (approximately 15 µA, **Figure 4**) and the one given by the Au@Pt/Au NPs/anti-p53 conjugate after reaction with the p53 immobilized on the magnetic beads (approximately 4 µA, "blank" assay in **Figure 5B**) is probably due to two different factors. First, as stated in the discussion of **Figure 3**, a decrease in the electrocatalytic activity of the NPs is observed after bioconjugation. This decrease could be attributed to a partial blocking of the Au surface by the antibodies, which might somehow affect the synergy between both metals. So, the current recorded for an Au@Pt/Au NPs/anti-p53 suspension is expected to be lower than that of the same amount of unmodified Au@Pt/Au NPs. Furthermore, the conditions of the assay are totally different in both cases. In the NPs quantification study, the $9.00x10^{14}$ NPs/mL suspension is directly deposited on the electrode surface. However, after the immunoassay is expected that not all the NPs are linked to the magnetic beads, something common in this kind of assays. Moreover, probably the presence of the magnetic beads on the electrode surface is also somehow hindering the WOR, contributing to a decrease in the current.

The specificity of the electrochemical immunoassay against other proteins present in human plasma, such as human IgG, was demonstrated. As shown in **Figure 5B**, the "blank" signal was not altered in presence of concentrations of human IgG as high as 500 nM ("negative control"). The same concentration of conformationally altered p53 ("positive") gave a high decrease in the analytical signal, demonstrating the selectivity of the method for the target protein.

Finally, dose-response experiments were performed using concentrations of conformationally altered p53 in the range between 50 - 1000 nM. The results obtained are depicted in Figure 5C and show that that the catalytic current decreases as the concentration of the analyte increases, as expected from the competitive immunoassay. This is adjusted to a linear relationship (r= 0.9955) according to the following equation:

$$Current_{300s}\ (nA) = -1.50\ [p53]\ (nM) + 3542$$

The LOD for conformationally altered p53, calculated as three times the standard deviation of the intercept divided by the slope, was 66 nM. The method showed an excellent reproducibility, with a RSD below the 5% (obtained for 3 repetitive assays for all the concentrations tested). These levels are close to the required for diagnostics applications [52] and also to those achieved using alternative approaches based on enzyme-linked immunosorbent assays (ELISA) [53], surface plasmon resonance (SPR) [54] and electrochemical impedance spectroscopic experiments (EIS) [55]. Moreover, our method presents clear advantages in terms of simplicity and analysis time, without the need of additional reagents after the immunoreaction. Work in progress in our lab is focused on the evaluation of different bifunctional NP structure/morphology so as to improve the sensitivity of the assay.

Conformationally altered p53 analysis in human plasma samples: spike and recovery

Analysis in real samples with minimal sample preparation is the main goal for demonstrating the good performance of the proposed analysis method in a real scenario. Spike and recovery experiment in human plasma samples from a cognitively healthy subject was performed as detailed at the experimental section, and the results are summarized in Table 1. The high recovery rate of the analytical signal, at levels around 90%, demonstrated that our methodology was not significantly affected by the real matrix, opening the way to an accurate determination of conformationally altered p53 in samples from Alzheimer's disease patients.

Table 1. Spike and recovery assay data. The study was done by spiking 100, 500 and 1000 nM of conformationally altered p53 in a plasma sample from a cognitively healthy subject (n=3 for each sample) and calculating the % recovery of the analytical signal when compared with the results in 0.1 M PBS pH 7.2.

Sample	Spiked conformationally altered p53 (nM)	Current in PBS (nA)	Current in real sample (nA)	Recovery (%)
Plasma from cognitively healthy subject	100	3356.80	2993.33	89.17
	500	2776.67	2533.82	91.25
	1000	2136.55	1970.00	92.20

CONCLUSIONS

In this work, we report for the first time the study and evaluation of the electrocatalytic activity of bifunctional core@shell Au@Pt/Au NPs towards the water oxidation reaction (WOR), together with their application as novel tags for the determination of an Alzheimer's disease biomarker in human plasma samples. Studies carried out with the different metallic NPs obtained during the successive steps of the synthetic procedure evidence the high catalytic activity of Pt compared with Au. Interestingly, a synergistic effect between both metals is observed when they are combined in the surface of the final Au@Pt/Au NPs. The presence of Au protuberances on the Pt shell also allows the easy immobilization of antibodies for the later application as tags in immunosensing.

Both the Au@Pt/Au NP tags and the electrocatalytic detection method based on the chronoamperometric monitoring of the WOR process present remarkable advantages compared to previously reported strategies based on other electroactive/electrocatalytic tags. On the one hand, the NP structure with a big Pt area and the small Au protuberances combines the excellent catalytic activity of Pt with the outstanding bioconjugation abilities of Au. Moreover, the detection method is performed in the same medium of the immunoreaction, avoiding additional experimental steps and the use of acidic and hazardous reagents usually required for electrochemical detection of other NP tags.

These advantages pave the way to future applications in fully integrated sensing platforms, such as lab-on-a-chip or lateral flow ones. In this line, the strong violet colour of Au@Pt/Au NP suspensions (maximum of absorbance at approx. 550 nm) allows to postulate these NPs as tags for dual electrochemical/optical detection in i.e. lateral flow assays. It's also worthy to mention the surface-enhanced Raman scattering (SERS) properties previously observed for such Au@Pt/Au NPs [45] which together with our findings make these NPs powerful tags with multidetection abilities.

AUTHOR INFORMATION

Corresponding Author

* Dr. Alfredo de la Escosura-Muñiz, Phone: +34 98 510 35 21,
E-mail address: alfredo.escosura@uniovi.es.

Author Contributions

The manuscript was written through contributions of all authors. All authors have given approval to the final version of the manuscript.

ACKNOWLEDGMENT

This work has been supported by the FC-GRUPIN-ID/2018/000166 project from the Asturias Regional Government and the CTQ2017–86994-R project from the Spanish Ministry of Economy and Competitiveness (MINECO). A. Iglesias-Mayor thanks the Spanish Ministry of Education, Culture and Sports (MECD) for the award of a FPU Grant (FPU2014/04686). O. Amor-Gutiérrez and A. de la Escosura-Muñiz thank the University of Oviedo for the "Plan de Apoyo y Promoción de la Investigación" grant (PAPI-18-PF-13) and the "Ayudas Proyectos Emergentes 2019" project (PAPI-19-EMERG-17), respectively. A. de la Escosura-Muñiz also acknowledges the Spanish Ministry of Science and Innovation MICINN (Spain) for the "Ramón y Cajal" Research Fellow (RyC-2016-20299).

REFERENCES

(1) Sharma, N.; Ojha, H.; Bharadwaj, A.; Pathak, D. P.; Sharma, R. K. Preparation and Catalytic Applications of Nanomaterials: A Review. *RSC Adv.* **2015**, *5* (66), 53381–53403. https://doi.org/10.1039/c5ra06778b.

(2) Reier, T.; Oezaslan, M.; Strasser, P. Electrocatalytic Oxygen Evolution Reaction (OER) on Ru, Ir, and Pt Catalysts: A Comparative Study of Nanoparticles and Bulk Materials. *ACS Catal.* **2012**, *2* (8), 1765–1772. https://doi.org/10.1021/cs3003098.

(3) Huang, Y.; Ren, J.; Qu, X. Nanozymes: Classification, Catalytic Mechanisms, Activity Regulation, and Applications. *Chem. Rev.* **2019**, *119* (6), 4357–4412. https://doi.org/10.1021/acs.chemrev.8b00672.

(4) Wu, J.; Wang, X.; Wang, Q.; Lou, Z.; Li, S.; Zhu, Y.; Qin, L.; Wei, H. Nanomaterials with Enzyme-like Characteristics (Nanozymes): Next-Generation Artificial Enzymes (II). *Chem. Soc. Rev.* **2019**, *48* (4), 1004–1076. https://doi.org/10.1039/c8cs00457a.

(5) Lin, Y.; Ren, J.; Qu, X. Catalytically Active Nanomaterials: A Promising Candidate for Artificial Enzymes. *Acc. Chem. Res.* **2014**, *47* (4), 1097–1105. https://doi.org/10.1021/ar400250z.

(6) Zhou, Y.; Liu, B.; Yang, R.; Liu, J. Filling in the Gaps between Nanozymes and Enzymes: Challenges and Opportunities. *Bioconjug. Chem.* **2017**, *28* (12), 2903–2909. https://doi.org/10.1021/acs.bioconjchem.7b00673.

(7) de la Escosura-Muñiz, A.; Ambrosi, A.; Merkoçi, A. Electrochemical Analysis with Nanoparticle-Based Biosystems. *TrAC - Trends Anal. Chem.* **2008**, *27* (7), 568–584. https://doi.org/10.1016/j.trac.2008.05.008.

(8) de la Escosura-Muñiz, A.; Merkoçi, A. Electrochemical Detection of Proteins Using Nanoparticles: Applications to Diagnostics. *Expert Opin. Med. Diagn.* **2010**, *4* (1), 21–37. https://doi.org/10.1517/17530050903386661.

(9) de la Escosura-Muñiz, A.; Parolo, C.; Merkoçi, A. Immunosensing Using Nanoparticles. *Mater. Today* **2010**, *13* (7–8), 24–34. https://doi.org/10.1016/S1369-7021(10)70125-5.

(10) Tian, L.; Liu, L.; Li, Y.; Wei, Q.; Cao, W. Ultrasensitive Sandwich-Type Electrochemical Immunosensor Based on Trimetallic Nanocomposite Signal Amplification Strategy for the Ultrasensitive Detection of CEA. *Sci. Rep.* **2016**, *6* (January), 30849. https://doi.org/10.1038/srep30849.

(11) Yang, Y.; Yan, Q.; Liu, Q.; Li, Y.; Liu, H.; Wang, P.; Chen, L.; Zhang, D. An Ultrasensitive Sandwich-Type Electrochemical Immunosensor Based on the Signal Amplification Strategy of Echinoidea-Shaped Au @ Ag-Cu2O Nanoparticles for Prostate Specific Antigen Detection. *Biosens. Bioelectron.* **2018**, *99* (August 2017), 450–457.

https://doi.org/10.1016/j.bios.2017.08.018.
(12) Iglesias-Mayor, A.; Amor-Gutiérrez, O.; Costa-García, A.; de la Escosura-Muñiz, A. Nanoparticles as Emerging Labels in Electrochemical Immunosensors. *Sensors* **2019**, *19*, 5137.
(13) Ambrosi, A.; Castañeda, M. T.; Killard, A. J.; Smyth, M. R.; Alegret, S.; Merkoçi, A. Double-Codified Gold Nanolabels for Enhanced Immunoanalysis. *Anal. Chem.* **2007**, *79* (14), 5232–5240. https://doi.org/10.1021/ac070357m.
(14) Ambrosi, A.; Airò, F.; Merkoçi, A. Enhanced Gold Nanoparticle Based ELISA for a Breast Cancer Biomarker. *Anal. Chem.* **2010**, *82* (3), 1151–1156. https://doi.org/10.1021/ac902492c.
(15) Luo, X.; Morrin, A.; Killard, A. J.; Smyth, M. R. Application of Nanoparticles in Electrochemical Sensors and Biosensors. *Electroanalysis* **2006**, *18* (4), 319–326. https://doi.org/10.1002/elan.200503415.
(16) Dequaire, M.; Degrand, C.; Limoges, B. An Electrochemical Metalloimmunoassay Based on a Colloidal Gold Label. *Anal. Chem.* **2000**, *72* (22), 5521–5528.
(17) Maltez-da Costa, M.; de la Escosura-Muñiz, A.; Merkoçi, A. Electrochemical Quantification of Gold Nanoparticles Based on Their Catalytic Properties toward Hydrogen Formation: Application in Magnetoimmunoassays. *Electrochem. commun.* **2010**, *12* (11), 1501–1504. https://doi.org/10.1016/j.elecom.2010.08.018.
(18) de la Escosura-Muñiz, A.; Maltez-da Costa, M.; Sánchez-Espinel, C.; Díaz-Freitas, B.; Fernández-Suarez, J.; González-Fernández, Á.; Merkoçi, A. Gold Nanoparticle-Based Electrochemical Magnetoimmunosensor for Rapid Detection of Anti-Hepatitis B Virus Antibodies in Human Serum. *Biosens. Bioelectron.* **2010**, *26* (4), 1710–1714. https://doi.org/10.1016/j.bios.2010.07.069.
(19) Maltez-da Costa, M.; de la Escosura-Muñiz, A.; Nogués, C.; Barrios, L.; Ibáñez, E.; Merkoçi, A. Simple Monitoring of Cancer Cells Using Nanoparticles. *Nano Lett.* **2012**, *12* (8), 4164–4171. https://doi.org/10.1021/nl301726g.
(20) de La Escosura-Muñiz, A.; Sánchez-Espinel, C.; Díaz-Freitas, B.; González-Fernández, Á.; Maltez-da Costa, M.; Merkoçi, A. Rapid Identification and Quantification of Tumor Cells Using an Electrocatalytic Method Based on Gold Nanoparticles. *Anal. Chem.* **2009**, *81* (24), 10268–10274. https://doi.org/10.1021/ac902087k.
(21) Hassan, A.-R. H. A.-A.; de la Escosura-Muñiz, A.; Merkoçi, A. Highly Sensitive and Rapid Determination of Escherichia Coli O157:H7 in Minced Beef and Water Using Electrocatalytic Gold Nanoparticle Tags. *Biosens. Bioelectron.* **2015**, *67* (15 May 2015), 511–515. https://doi.org/10.1016/j.bios.2014.09.019.
(22) de la Escosura-Muñiz, A.; Plichta, Z.; Horák, D.; Merkoçi, A. Alzheimer′s Disease Biomarkers Detection in Human Samples by Efficient Capturing through Porous Magnetic Microspheres and Labelling with Electrocatalytic Gold Nanoparticles. *Biosens. Bioelectron.* **2015**, *67* (15 May 2015), 162–169. https://doi.org/10.1016/j.bios.2014.07.086.
(23) Baptista-Pires, L.; de la Escosura-Muñiz, A.; Balsells, M.; Zuaznabar-Gardona, J. C.; Merkoçi, A. Production and Printing of Graphene Oxide Foam Ink for Electrocatalytic Applications. *Electrochem. commun.* **2019**, *98* (January 2019), 6–9. https://doi.org/10.1016/j.elecom.2018.11.001.
(24) Li, P.; Zhao, R.; Chen, H.; Wang, H.; Wei, P.; Huang, H.; Liu, Q.; Li, T.; Shi, X.; Zhang, Y.; Liu, M.; Sun, X. Recent Advances in the Development of Water Oxidation Electrocatalysts at Mild PH. *Small* **2019**, *15* (13), 1805103. https://doi.org/10.1002/smll.201805103.
(25) Dau, H.; Limberg, C.; Reier, T.; Risch, M.; Roggan, S.; Strasser, P. The Mechanism of Water Oxidation: From Electrolysis via Homogeneous to Biological Catalysis. *ChemCatChem* **2010**, *2* (7), 724–761. https://doi.org/10.1002/cctc.201000126.
(26) McCrory, C. C. L.; Jung, S.; Ferrer, I. M.; Chatman, S. M.; Peters, J. C.; Jaramillo, T. F. Benchmarking Hydrogen Evolving Reaction and Oxygen Evolving Reaction Electrocatalysts for Solar Water Splitting Devices. *J. Am. Chem. Soc.* **2015**, *137* (13), 4347–4357. https://doi.org/10.1021/ja510442p.
(27) Jamesh, M. I. Recent Progress on Earth Abundant Hydrogen Evolution Reaction and Oxygen Evolution Reaction Bifunctional Electrocatalyst for Overall Water Splitting in Alkaline Media. *J. Power Sources* **2016**, *333* (30 November 2016), 213–236. https://doi.org/10.1016/j.jpowsour.2016.09.161.
(28) Jamesh, M. I.; Xiaoming, S. Recent Progress on Earth Abundant Electrocatalysts for Oxygen Evolution Reaction (OER) in Alkaline Medium to Achieve Efficient Water Splitting – A Review. *J. Power Sources* **2018**, *400* (1 October 2018), 31–68. https://doi.org/10.1016/j.jechem.2018.09.016.
(29) Blakemore, J. D.; Crabtree, R. H.; Brudvig, G. W. Molecular Catalysts for Water Oxidation. *Chem. Rev.* **2015**, *115* (23), 12974–13005. https://doi.org/10.1021/acs.chemrev.5b00122.
(30) Rivas, L.; de la Escosura-Muñiz, A.; Pons, J.; Merkoçi, A. Alzheimer Disease Biomarker Detection Through Electrocatalytic Water Oxidation Induced by Iridium Oxide Nanoparticles. *Electroanalysis* **2014**, *26* (6), 1287–1294. https://doi.org/10.1002/elan.201400027.
(31) Quesada-González, D.; Baiocco, A.; Martos, A. A.; de la Escosura-Muñiz, A.; Palleschi, G.; Merkoçi, A. Iridium Oxide (IV) Nanoparticle-Based Electrocatalytic Detection of PBDE. *Biosens. Bioelectron.* **2019**, *127* (15 February 2019), 150–154. https://doi.org/10.1016/j.bios.2018.11.050.
(32) Chen, J.; Lim, B.; Lee, E. P.; Xia, Y. Shape-Controlled Synthesis of Platinum Nanocrystals for Catalytic and Electrocatalytic Applications. *Nano Today* **2009**, *4* (1), 81–95. https://doi.org/10.1016/j.nantod.2008.09.002.
(33) Chen, A.; Holt-Hindle, P. Platinum-Based Nanostructured Materials : Synthesis , Properties , and Applications. *Chem. Rev.* **2010**, *110* (6), 3767–3804. https://doi.org/10.1021/cr9003902.
(34) Zhao, D.; Xu, B.-Q. Enhancement of Pt Utilization in Electrocatalysts by Using Gold Nanoparticles. *Angew. Chemie Int. Ed.* **2006**, *45* (30), 4955–4959. https://doi.org/10.1002/anie.200600155.
(35) Wang, A.; Liu, X. Y.; Mou, C.-Y.; Zhang, T. Understanding the Synergistic Effects of Gold Bimetallic Catalysts. *J. Catal.* **2013**, *308* (December 2013), 258–271. https://doi.org/10.1016/j.jcat.2013.08.023.
(36) Tang, J.; Tang, D. Non-Enzymatic Electrochemical Immunoassay Using Noble Metal Nanoparticles: A Review. *Microchim. Acta* **2015**, *182* (October 2015), 2077–2089. https://doi.org/10.1007/s00604-015-1567-8.
(37) Notar Francesco, I.; Fontaine-Vive, F.; Antoniotti, S. Synergy in the Catalytic Activity of Bimetallic Nanoparticles and New Synthetic Methods for the Preparation of Fine Chemicals. *ChemCatChem* **2014**, *6* (10), 2784–2791. https://doi.org/10.1002/cctc.201402252.
(38) Sha, J.; Paul, S.; Dumeignil, F.; Wojcieszak, R. Au-Based Bimetallic Catalysts: How the Synergy between Two Metals Affects Their Catalytic Activity. *RSC Adv.* **2019**, *9* (51), 29888–29901. https://doi.org/10.1039/c9ra06001d.
(39) Ataee-Esfahani, H.; Wang, L.; Nemoto, Y.; Yamauchi, Y. Synthesis of Bimetallic Au@Pt Nanoparticles with Au Core and Nanostructured Pt Shell toward Highly Active Electrocatalysts. *Chem. Mater.* **2010**, *22* (23), 6310–6318. https://doi.org/10.1021/cm102074w.
(40) Zhang, G.-R.; Zhao, D.; Feng, Y.-Y.; Zhang, B.; Su, D. S.; Liu, G.; Xu, B.-Q. Catalytic Pt-on-Au Nanostructures : Why Pt Becomes More Active on Smaller Au Particles. *ACS Nano* **2012**, *6* (3), 2226–2236. https://doi.org/10.1021/nn204378t.
(41) Wang, R.; Wang, A.-J.; Liu, W.-D.; Yuan, P.-X.; Xue, Y.; Luo, X.; Feng, J.-J. A Novel Label-Free Electrochemical Immunosensor for Ultra-Sensitively Detecting Prostate Specific Antigen Based on the Enhanced Catalytic Currents of Oxygen Reduction Catalyzed by Core-Shell Au@Pt Nanocrystals. *Biosens. Bioelectron.* **2018**, *102* (15 April 2018), 276–281. https://doi.org/10.1016/j.bios.2017.11.041.
(42) Wang, A.-J.; Zhu, X.-Y.; Chen, Y.; Luo, X.; Xue, Y.; Feng, J.-J. Ultrasensitive Label-Free Electrochemical Immunoassay of Carbohydrate Antigen 15-3 Using Dendritic Au@Pt Nanocrystals/Ferrocene-Grafted-Chitosan for Efficient Signal Amplification. *Sensors Actuators B Chem.* **2019**, *292* (1 August 2019), 164–170. https://doi.org/10.1016/j.snb.2019.04.128.
(43) Chen, Y.; Ge, X.-Y.; Cen, S.-Y.; Wang, A.-J.; Luo, X.; Feng, J.-J. Ultrasensitive Dual-Signal Ratiometric Electrochemical Aptasensor for Neuron-Specific Enolase Based on Au Nanoparticles@Pd Nanoclusters-Poly(Bismarck Brown Y) and Dendritic AuPt Nanoassemblies. *Sensors Actuators B Chem.* **2020**, *311* (15 May 2020), 127931. https://doi.org/10.1016/j.snb.2020.127931.

(44) Zhu, F.; Zhao, G.; Dou, W. Electrochemical Sandwich Immunoassay for Escherichia Coli O157:H7 Based on the Use of Magnetic Nanoparticles and Graphene Functionalized with Electrocatalytically Active Au@ Pt Core/Shell Nanoparticles. *Microchim. Acta* **2018**, *185* (10), 455. https://doi.org/10.1007/s00604-018-2984-2.

(45) Xie, W.; Herrmann, C.; Kömpe, K.; Haase, M.; Schlücker, S. Synthesis of Bifunctional Au/Pt/Au Core/Shell Nanoraspberries for in Situ SERS Monitoring of Platinum-Catalyzed Reactions. *J. Am. Chem. Soc.* **2011**, *133* (48), 19302–19305. https://doi.org/10.1021/ja208298q.

(46) Li, X.-R.; Xu, M.-C.; Chen, H.-Y.; Xu, J.-J. Bimetallic Au@Pt@Au Core-Shell Nanoparticles on Graphene Oxide Nanosheets for High-Performance H202 Bi-Directional Sensing. *J. Mater. Chem. B* **2015**, *3* (21), 4355–4362. https://doi.org/10.1039/c5tb00312a.

(47) Prince, M.; Comas-Herrera, A.; Knapp, M.; Guerchet, M.; Karagiannidou, M. *World Alzheimer Report 2016 Improving Healthcare for People Living with Dementia. Coverage, Quality and Costs Now and in the Future*; 2016.

(48) Lanni, C.; Uberti, D.; Racchi, M.; Govoni, S.; Memo, M. Unfolded P53: A Potential Biomarker for Alzheimer's Disease. *J. Alzheimer's Dis.* **2007**, *12* (1), 93–99. https://doi.org/10.3233/JAD-2007-12109.

(49) Tonello, S.; Stradolini, F.; Abate, G.; Uberti, D.; Serpelloni, M.; Carrara, S.; Sardini, E. Electrochemical Detection of Different P53 Conformations by Using Nanostructured Surfaces. *Sci. Rep.* **2019**, *9*, 17347. https://doi.org/10.1038/s41598-019-53994-6.

(50) Turkevich, J.; Stevenson, P. C.; Hillier, J. A Study of the Nucleation and Growth Processes in the Synthesis of Colloidal Gold. *Discuss. Faraday Soc.* **1951**, *11*, 55–75. https://doi.org/10.1039/DF9511100055.

(51) Maltez-Da Costa, M.; De La Escosura-Muñiz, A.; Nogués, C.; Barrios, L.; Ibáñez, E.; Merkoçi, A. Detection of Circulating Cancer Cells Using Electrocatalytic Gold Nanoparticles. *Small* **2012**, *8* (23), 3605–3612. https://doi.org/10.1002/smll.201201205.

(52) Arce-Varas, N.; Abate, G.; Prandelli, C.; Martínez, C.; Cuetos, F.; Menéndez, M.; Marziano, M.; Cabrera-García, D.; Fernández-Sánchez, M. T.; Novelli, A.; Memo, M.; Uberti, D. Comparison of Extracellular and Intracellular Blood Compartments Highlights Redox Alterations in Alzheimer's and Mild Cognitive Impairment Patients. *Curr. Alzheimer Res.* **2017**, *14* (1), 112–122. https://doi.org/10.2174/1567205013666161010125413.

(53) Jagelská, E.; Brázda, V.; Pospisilová, S.; Vojtesek, B.; Palecek, E. New ELISA Technique for Analysis of P53 Protein/DNA Binding Properties. *J. Immunol. Methods* **2002**, *267* (2), 227–235. https://doi.org/10.1016/S0022-1759(02)00182-5.

(54) Wang, Y.; Zhu, X.; Wu, M.; Xia, N.; Wang, J.; Zhou, F. Simultaneous and Label-Free Determination of Wild-Type and Mutant P53 at a Single Surface Plasmon Resonance Chip Preimmobilized with Consensus DNA and Monoclonal Antibody. *Anal. Chem.* **2009**, *81* (20), 8441–8446. https://doi.org/10.1021/ac9014269.

(55) Yeo, J.; Park, J.-Y.; Won, J. B.; Yoon, S. L.; Byeang, H. K.; Cho, Y.; Park, S.-M. Label-Free Electrochemical Detection of the P53 Core Domain Protein on Its Antibody Immobilized Electrode. *Anal. Chem.* **2009**, *81* (12), 4770–4777. https://doi.org/10.1021/ac900301h.

Table of contents: